PAPER

Check for updates

MnFe₂O₄@SiO₂@CeO₂ core−shell nanostructures for applications in water remediation†

Garret Dee, [a] Hend Shayoub,[a] Helen McNeill,[a] Itziar Sánchez Lozano,[b] Aran Rafferty [a] and Yurii K. Gun'ko *[a]

Removal of dye pollutants from wastewater is among the most important emerging needs in environmental science and engineering. The main objective of our work is to develop new magnetic core−shell nanostructures and explore their use for potential removal of pollutants from water using an external magnetic field. Herein, we have prepared magnetic core−shell nanoparticles that demonstrated excellent dye pollutant adsorbent properties. These nanoparticles are composed of a manganese ferrite magnetic core coated with silica, to protect the core and enable further functionalisation, then finally coated with ceria, which is shown to be an effective adsorbent. The magnetic core−shell nanostructures have been synthesized by a modification of solvothermal synthesis. The nanoparticles were fully characterised at each stage of the synthesis by powder X-ray diffraction (pXRD), transmission electron microscopy (TEM), vibrating sample magnetometry (VSM) and Fourier transform infrared spectroscopy (FTIR). These particles were found to be effective in removing methylene blue (MB) dye from water, which was validated by UV-visible (UV-vis) spectroscopy. These particles can be quickly removed from solution using a permanent magnet and then can be recycled after being placed in the furnace at 400 °C to burn off any organic residues. The particles were found to retain their ability to adsorb the pollutant after several cycles and TEM images of the particles after several cycles showed no change in the morphology. This research demonstrated the capacity of magnetic core−shell nanostructures to be used for water remediation.

Introduction

The area of waste water remediation[1] is one of the most important emerging fields in science and technology, as population growth, urbanization and industrialisation have all put pressure on clean water sources. Dyes are one of the major pollutants in the wastewater coming from industries such as the textile and printing industry.[2] Dyes in wastewater can be very harmful to the aquatic environment and can be dangerous to people by causing allergic reactions and skin irritation.[3] Methylene blue (MB) is one of the dyes that is used in the textile and printing industries. It has previously been reported that people exposed to MB through wastewater in the environment have

experienced nausea, headaches and chest pains with infants and pregnant women being particularly susceptible.[4]

Many innovative technologies have been developed for removal of dyes from wastewater. These include but are not limited to ultra- and nano-filtration,[5] photocatalytic degradation,[6] ion exchange,[7] electrochemical techniques,[8] ozone degradation,[9] metal oxide degradation[10] and adsorption.[11] Other methods involve the degradation of dyes, which increase the number of products in the system and so may limit the effectiveness of a method to remove the degradation products. Adsorption removal techniques do not suffer from this effect, as the pollutant is not changed upon adsorption on to the surface of the material. Manganese dioxide and manganese dioxide coated magnetic nanoparticles have been studied for MB dye removal previously with conflicting reports regarding the mechanism with one reporting degradation,[10] while another is reporting adsorption.[2]

Magnetic nanoparticles (MNPs) have been extensively explored over many years due to their unique properties. These properties have found application in magnetic separation,[12] magnetic targeted drug delivery,[13] magnetic resonance imaging (MRI) diagnostics[14] and magnetic heating in cancer hyperthermia therapy.[15] MNPs can be prepared by various methods which include coprecipitation,[16] thermal decomposition[17] and

aSchool of Chemistry, University of Dublin, Trinity College, Dublin 2, Ireland. E-mail: igounko@tcd.ie

bFacultad de Ciencias Químicas, Universidad de Alcalá de Henares, Spain

thermal synthesis.[18] Previously, a significant amount of work has been done in developing core@shell MNPs with the magnetic functionality at the core.[19] By putting an adsorbent or catalytic layer on the surface of a magnetic nanoparticle, pollutants could be removed or degraded and then the nanocomposite can be magnetically extracted from the solution. This has been achieved previously for manganese oxide (MnO_2) shells which has both an adsorbent[2] and degradation effect.[20] Cerium dioxide it a well know catalytic oxide for its use in catalytic converters in combustion engine transportation vehicles.[21] Cerium dioxide has also been explored as an adsorbent for small gaseous molecules,[22] toxic metal ions in composite materials[23] and for removal of azo dyes on immobilized surfaces.[24]

In this work, cerium dioxide was deposited on the surface of silica coated magnetic nanoparticles forming new core–shell nanocomposites. The nanocomposite particles were characterized by various instrumental techniques and then they were tested for the methylene blue dye removal. It was found that these dye-adsorbed particles could be magnetically extracted from solution with subsequent regeneration at 400 °C to burn off the adsorbed dye. After regeneration the particles could then be used again for further dye removal. The nanocomposite particles were found to be highly effective in dye removal even after several recycles.

Results and discussion

Preparation of the manganese ferrite magnetic core nanoparticles

The manganese ferrite ($MnFe_2O_4$) magnetic cores were synthesised by mixing the precursors in the polyol solvent such as ethylene glycol and refluxing, as described in the Experimental section. This synthesis, which is a modification of the solvothermal method,[18] is known to produce nanoparticles with a larger size than the coprecipitation route. When nanoparticles of small particle size (<20 nm) that are synthesized using coprecipitation are coated with silica, it results in coagulation of the silica, causing fusing between particles and the formation of multicore particles.[25] These larger nanoparticles were synthesised for this work to avoid excessive agglomeration and so produce individual coated nanoparticles with high magnetic moments.

TEM images (Fig. 1) showed that the synthesis had produced particles with a size of 100 ± 20 nm, giving a sample with a narrow size range. The particles can be seen to be composed of grains that have been fused to give the larger nanoparticles (Fig. S1†), which is consistent with similar previous work.[26] VSM analysis (Fig. S2†) of the sample gave a saturation magnetisation of 60 Am² kg⁻¹ at 1 T. The sample reached saturation magnetisation quickly and there was no sign of coercivity or remanence in the hysteresis loop, indicating superparamagnetic behaviour. The particles could be easily extracted from solution with a neodymium magnet. XRD analysis (Fig. S3†) gave a match for manganese ferrite (JCPDS 10-0319) with no other phases showing. The samples showed lattice contraction to the matched reference card ($a_{reference}$ =
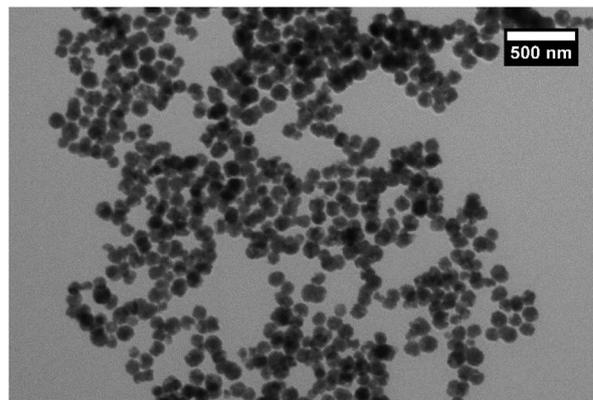

Fig. 1 TEM image of the synthesised manganese ferrite core nanoparticles.

0.84990 nm, a_{sample} = 0.75221 nm) when the peaks were analysed by graphing $1/d^2$ against $h^2 + k^2 + l^2$ for each peak to get the lattice constant (Fig. S4†). This can be rationalised by the particles being composed of grains which have smaller size and therefore more lattice contraction and surface stress[27] and also the possibility of nonstoichiometric manganese ferrite.[28] This effect is visible in the shifting of the peaks in the XRD to the right from the reference pattern while still matching the pattern. Analysis of the pattern using Bruker software gave crystallite size of 9.3 nm, which is consistent with the grain structure of the larger particles. The broadening of the peaks is attributed to the small size of the grains that make up the particles, consistent with the concepts of Scherrer.[29] FTIR spectra of the sample (Fig. S5†) showed the typical peak at 535 cm⁻¹ corresponding to metal–O stretching modes of tetrahedral and octahedral sites.[30] The other small peaks at 1579, 1354, *etc.* could be from the acetate that was used in the reaction and would bind through the carboxylate to the surface of the ferrite.

Stabilisation of the magnetic cores with citrate

The manganese ferrite particles were then stabilised with citrate ions prior to silica coating as it was found the citrate functionalisation prior to silica coating gave better results. This concept follows previous work with some modifications.[31,32] For coating the cores with silica, it is best that the particles are dispersed and not agglomerating in solution. Agglomeration causes fusing of the silica shell and not the formation of individual silica coated particles. The acetate used in the synthesis stabilises the particles in solution as evidenced by DLS measurements over one week, but citrate stabilisation gave a better result (Table S1†). The count rate for the magnetic cores reduced by 88% over 7 days while the count rate for the citrate-stabilised cores reduced by 64% over 7 days, indicating an increase in stability over that time compared with the cores. From the DLS analysis of the manganese ferrite cores, we see the Z-average and the PDI of the core changes a lot over time due to agglomeration and then losing colloidal stability to precipitate out of solution. For the citrate-stabilised cores, the Z-

average decreases slightly and the PDI is stable over the 7 days. This indicates that the citrate-stabilised cores are not agglomerating and have higher colloidal stability.

FTIR analysis (Fig. S5†) of the citrate-stabilised cores showed the characteristic peaks for citrate at 1580 and 1390 cm^{-1}, from the symmetric and asymmetric stretching of the –COOH.[33] VSM analysis (Fig. S2†) demonstrated a reduction in magnetisation to 58 Am^2 kg^{-1} while still having the same profile as the core MNP precursor, showing that it reached saturation magnetisation quickly and there was no sign of coercivity or remanence in the hysteresis loop. XRD analysis (Fig. S6†) showed no changes in the peaks positions with a match for the phase as before. The crystallite size reduced to 9.0 nm with the citrate coating. TEM images of the citrate-stabilised cores (Fig. S7†) showed no change is morphology as expected but the particles were dispersed with less agglomeration. These particles could still be extracted from solution with a neodymium magnet in under 3 hours, but the extraction was not as quick as with the unstabilised manganese ferrite cores.

Coating the magnetic cores with silica

The silica coating have been produced by the Stober method[34] which is a well-established process for coating of magnetic nanoparticles. The Stober method[34] for formation of silica (silicon dioxide or SiO$_2$) which was first introduced by Philipse to coat magnetic ferrites[35] is well established as an effective way to coat magnetic ferrites with many modifications in the literature.[31,36,37] Following this method, our citrate-stabilised magnetic cores were coated with a layer of silica. Using the average size of the cores from the TEM images previously and knowing the concentration of the MNP solution, as well as other properties from reference material, we were able to calculate the amount of TEOS precursor to create a shell of a certain thickness (eqn (S1)–(S3)†). For a calculated shell of 12.5 nm, our synthesis gave a shell of approximately 15 nm as can be seen in a TEM image (Fig. S8†). The nanocomposite particles were well separated with all particles coated and no agglomeration observed in the sample. The size was determined to be 130 ±

20 nm. This synthesis gave well-coated magnetic nanoparticles as can be seen in the TEM image (Fig. 2).

VSM analysis (Fig. S2†) showed a reduction in the saturation magnetisation to 35 Am^2 kg^{-1} as would be expected when adding a nonmagnetic layer to the magnetic cores. The profile of the hysteresis loop did not change with the saturation magnetisation being reached quickly and no sign of coercivity or remanence. XRD analysis (Fig. S9†) showed no significant change in the position or profiles of the peaks. The crystallite size calculation by the Bruker XRD software gave a size of 9.5 nm. A possible rationalisation for this result could be the silica shell may have relaxed the surface contraction and so the instrument observes larger crystallites. FTIR analysis (Fig. S5†) showed the expected peaks for silica in the spectrum at 1010 cm^{-1} for the Si–OH bond and the peak at 535 cm^{-1} for the metal–O bond of the spinel. DLS of the silica-coated nanocomposites (Table S1†) showed that the silica coating gave stabilisation to the particles comparable to the citrate-coated cores with a decrease of 65% over 7 days in the count rate. In addition, the Z-average and PDI do not vary considerably over the 7 days similar to the citrate-stabilised cores. Again, these nanocomposites could still be magnetically extracted from solution within 3 hours similar to the citrate-stabilised cores.

It is well know that mesoporous silica can be prepared by adding CTAB to the basic reaction solution prior to TEOS addition, which can then be calcined[38] or washed[39] to remove residue CTAB. The addition of a porous silica shell to improve adsorption is a possible modification that could be done as future work.

Coating the silica shell with a ceria layer

Ceria (cerium dioxide or CeO$_2$) was synthesised *in situ* with the silica-coated particles following a previously reported method[40] using Ce(NO$_3$)$_3$·6H$_2$O and hexamethylenetetramine (HMTA) as described in the Experimental section. A calculation could be done to estimate the thickness of shell that a certain amount of precursor will produce once certain properties are known. The measured and determined parameters include the size of the silica-coated precursor particles (from TEM images), the density of the silica-coated particles (from references and a calculation, see eqn (S4)†), the amount of the silica-coated precursor put into the reaction, the density of the second shell material (from references), and the molar masses of the materials and precursor, as done previously. TEM images (Fig. 3) of the particles after the synthesis confirmed that SiO$_2$ shells were coated with CeO$_2$. The particles showed little agglomeration with the size determined to be 145 ± 20 nm for a size distribution count of 100 particles.

This finding was in agreement for a calculated shell thickness of 5 nm. The shell was not as uniform as the silica shell as it was composed of small crystallites of the CeO$_2$ on the surface of the silica.

VSM analysis (Fig. S2†) showed a reduction in the magnetisation as expected from 35 Am^2 kg^{-1} for the precursor particles to 20 Am^2 kg^{-1} for the ceria coated product particles. The hysteresis loop demonstrated the same characteristics as
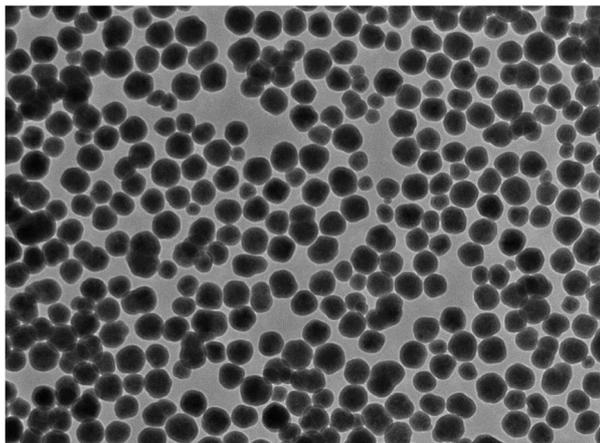

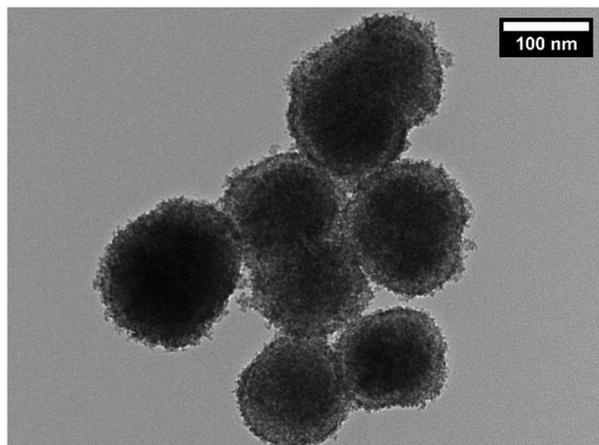**Fig. 2** TEM image of the SiO$_2$ coated MnFe$_2$O$_4$ magnetic core nanoparticles.

Fig. 3 TEM image of the MnFe$_2$O$_4$@SiO$_2$@CeO$_2$ particles.

pervious with the saturation magnetisation being reached quickly and no sign of coercivity or remanence. The particles could be magnetically removed from aqueous solution in three hours (Fig. S10†). XRD analysis (Fig. S11†) showed the presence of two phases for MnFe$_2$O$_4$ and CeO$_2$, with the MnFe$_2$O$_4$ peaks shifted slightly as they were in the precursor analysis discussed previously and the match for CeO$_2$. There was no other phases present indicating that only CeO$_2$ was attached to the surface. FTIR spectra (Fig. S5†) contained the same silica peaks as previously observed. The peak for the metal–O stretch of the ferrite was now occluded by the spectra for CeO$_2$ in that region.

In order to understand the surface area and pore size distribution characteristics of the synthesised ceria-coated magnetic nanoparticles, BET surface area analysis was performed. A surface area value of 136.7 m^2 g^{-1} was calculated from the adsorption branch of the isotherm (Fig. S12†) in the linear region (P/P_0: 0.1–0.3), which according to the BET model can be used to calculate the surface area.[41] The surface-to-volume ratio of nanoparticles is very high, relative to micrometer-sized particles, and therefore nanoparticles are expected to exhibit a relatively high surface area per unit mass, as is the case here. The adsorption–desorption isotherm was type IV, with hysteresis occurring in the approximate P/P_0 range: 0.35–0.75. The Barrett–Joyner–Halenda (BJH) method was used to calculate pore size and pore volume from the desorption branch of the isotherm where hysteresis occurred.[42] The pore size distribution is shown (Fig. S13†). The hysteresis observed can be attributed to the inter-particulate void spaces between the individual grains. As observed from the pore size distribution (Fig. S13†), a significant peak occurs at pore diameters below 5 nm with a mode value of 3.65 nm. The volume of the sub 5 nm void spaces is 0.08 cm^3 g^{-1} or 61.2% of the total pore volume. This suggests a narrow size distribution of the grains, which make up the particles, with the grains capable of packing and fitting together in a repeatable manner.

EDX analysis of the particles (Fig. S14†) showed that the nanocomposite contains Ce, Si, Fe and Mn. The carbon peak

also came from the holder. The percent atomic ratio for Mn + Fe : Si : Ce was found to be 44.68 : 24.53 : 30.79. This is consistent with a large MnFe$_2$O$_4$ core and thin SiO$_2$ and CeO$_2$ shells as seen in the TEM image (Fig. 3). The ratio of CeO$_2$ to the MnFe$_2$O$_4$@SiO$_2$ core could have an influence on the adsorption capacity in this system. It would also have an influence on the magnetisation value of the final nanocomposite, as higher ratios of CeO$_2$ would reduce the magnetisation. A possible future line of research would be varying the CeO$_2$ shell ratio to the MnFe$_2$O$_4$@SiO$_2$ core and quantifying the changes in adsorption and magnetisation.

It was also considered creating SiO$_2$@CeO$_2$ particles but then the magnetic extraction functionality would be lost, so these type of nanoparticles were not prepared.

Testing of the ceria coated magnetic nanoparticles for methylene blue dye removal from water

Methylene blue (MB) removal from water can be followed by UV-vis spectra of the absorbance band at 664 nm. Using the Beer–Lambert law, removal or degradation of MB from the solution can be quantified. Previous research has been conducted about the method by which MB is removed from water and the main concept of this research demonstrates that either a material behaves as an adsorbent to remove the dye or the catalytic degradation of the dye is caused by that material.[2,10] As a result, the experiments were conducted in the presence and absence of UV-vis light in order to determine which process is involved in the dye removal caused by the ceria-coated MNPs and to quantify the dye removal with these coated MNPs. A standard curve (Fig. S15†) determined the molar extinction coefficient (ε) and the concentration of the stock solution, which was calculated to be 24 μM.

Control experiments were done with the MB solution, where the solution was exposed to light from a Xenon lamp source over one hour while stirring and the absorbance measured to see the reduction in the MB concentration. The experiments involved the MB solution in a quartz reaction chamber and in borosilicate glass, which have a UV cut-off of <190 nm and 330 nm respectively (Fig. S16†). These explorations showed that MB was degraded by 6% by visible light above 360 nm (A) while it is degraded by 60% by light above 190 nm (B) as was evidenced by the UV-vis spectra of the two solutions over the hour (Fig. S17†).

A control experiment with the silica coated MNPs in borosilicate glass with the xenon light source was done to see the MB removal with these particles as the adsorbent (Fig. 4A). A calculation for these particles using this spectrum showed that 50 mg of these particles extracted 0.3 mg of MB from a 200 mL aqueous solution containing 8.9 mg L^{-1} (24 μM), giving a sorbent capacity of 6.9 mg g^{-1} for MB with the silica-coated nanoparticles at this concentration. The spectrum only indicated the particles acting as an adsorbent with no photocatalytic degradation because there is no change in MB concentration after 5 minutes.

The CeO$_2$ coated particles were then tested for removal of the MB solution in the borosilicate glass using the xenon light
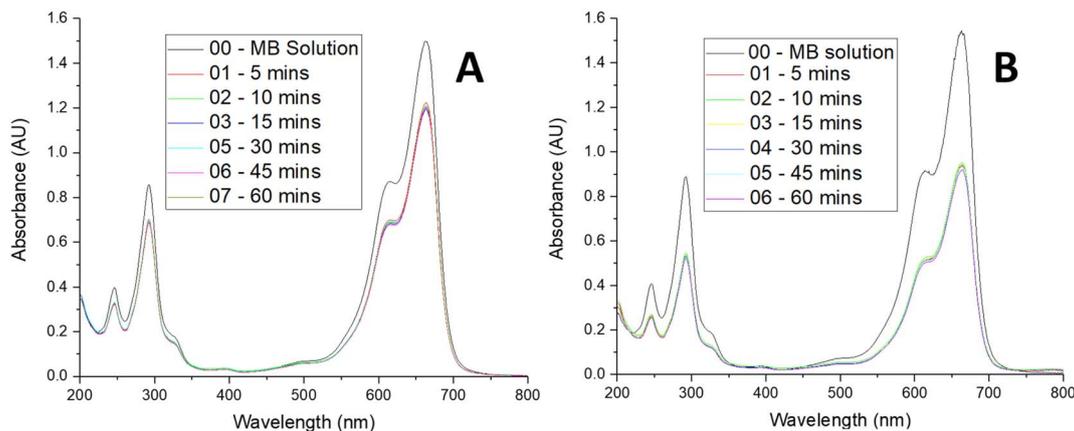
Fig. 4 UV–vis spectra showing (A) MB removal over 1 hour with SiO_2 coated MNPs, (B) MB removal over 1 hour with CeO_2 coated MNPs. 200 mL MB and 50 mg MNPs.

source. The UV-vis spectra of these experiments were taken over the hour to see the change is concentration of the MB (Fig. 4B). The borosilicate glass experiment demonstrated the ceria coated particles acting as an adsorbent, with the removal of the MB being greater than for the silica particles on their own. A calculation for these particles using the spectra showed that 50 mg of these particles extracted 0.7 mg of MB from a 200 mL aqueous solution containing 8.9 mg L^{-1} (24 μM), giving a sorbent capacity of 14.6 mg g^{-1} for MB with the ceria-coated nanoparticles at this concentration. Again, no photocatalytic degradation is observed, as the MB concentration remains constant once the adsorption has taken place over the first 5 minutes of the experiment.

One final experiment involved the CeO_2 coated particles being tested for MB removal in the cuvette of quartz glass using the xenon light source. The spectra for the experiment (Fig. S18†) showed both adsorbent and degradation processes taking place, where there is an initial large drop in the MB concentration after 5 minutes due to adsorption and a slow continuing reduction in the concentration during the hour due to photo-degradation.

Mass spectrometry of the MB solution before these reactions (Fig. S19†), after the borosilicate glass with the ceria-coated MNPs reaction (Fig. S20†) and after the quartz glass with the ceria-coated MNPs reaction (Fig. S21†) were taken. The MS analysis revealed that there is no change in the MB solution after the MNPs were extracted for the ceria adsorbed solution under light of >360 nm but there is a degradation product for the ceria adsorbed solution under light >190 nm. The most abundant ion, which has an m/z of 284, corresponds to the MB molecule in both spectra. Upon the exposure of the MB solution to the UV-vis light, a fragment with m/z of 270 was observed, which means that a photo-degradation intermediate was formed. The two methyl groups that are bonded to nitrogen groups in the MB structure are expected to have the lowest bond energy.[43] As a result, the first intermediate formed involves the demethylation of MB to form a compound that is known as azure B (Fig. S22†).[10] If MB was left under the exposure of UV-vis

light for a much longer period of time, it may have continued to degrade to form more intermediates which have been reported by previous research.[10] The formation of azure B accounts for the change in the absorption peak of the MB solution over time. These results verify the UV-vis analysis that the ceria-coated particles adsorb the MB blue and do not catalytically degrade it and that UV-light degrades MB, as discussed previously in this section.

These ceria coated magnetic nanoparticles were tested for MB removal using water as a model for potential application as a recyclable pollutant removal from wastewater. This was done because MB removal can be followed easily with UV-vis spectroscopy. Future studies will include using actual wastewater to quantify their efficacy in a real-world situation.

The magnetic functionality of the particles may also find application for activation of the adsorption effect[44] in addition to the magnetic extraction functionality.

Kinetics analysis of adsorption of MB onto the ceria coated particles

A study of the kinetics of adsorption was carried out at initial concentrations of 10, 6 and 2 mg L^{-1} of MB with the adsorption followed at time intervals until equilibrium had been reached, as describe in the Experimental section. The study of adsorption gives insights into the sorbate uptake rate. Information from the kinetics analysis can be used to understand the processes happening at the surface of the adsorbent according to various kinetic models. This information can be then used for further adsorption process design.[2] The data from the kinetics experiments were analysed for the pseudo-first-order and pseudo-second-order models.[45]

The pseudo-first-order kinetic model follows the rate equation

$$\frac{\mathrm{d}q(t)}{\mathrm{d}t} = k_1(q_e - q(t))$$

where $q(t)$ is the quantity of sorbate adsorbed at time t (mg g^{-1}), q_e is the quantity of sorbate adsorbed at equilibrium (mg g^{-1})

and k_1 is the rate constant (min^{-1}). This equation can be integrated with boundary conditions $q(t) = 0$ at $t = 0$ and $q(t) = q(t)$ at $t = t$ to give

$$q(t) = q_e(1 - e^{-k_1 t})$$

which can be linearized as shown previously[46] to the $y = mx + c$ form of

$$\ln[q_e - q(t)] = -k_1 t + \ln[q_e]$$

A plot of $\ln[q_e - q(t)]$ against t will give a slope of $-k_1$ and intercept of $\ln[q_e]$.

The pseudo-second-order kinetic model follows the rate equation

$$\frac{dq(t)}{dt} = k_2(q_e - q(t))^2$$

where k_2 is the rate constant ($\text{mg}^{-1}\ \text{g}\ \text{min}^{-1}$). This equation can be integrated with boundary conditions $q(t) = 0$ at $t = 0$ and $q(t) = q(t)$ at $t = t$ to give

$$q(t) = \frac{q_e^2 k_2 t}{1 + q_e k_2 t}$$

which can be linearized as shown previously[46] to the $y = mx + c$ form of

$$\frac{t}{q(t)} = \frac{1}{q_e} t + \frac{1}{k_2 q_e^2}$$

A plot of $\frac{t}{q(t)}$ against t will give a slope of $\frac{1}{q_e}$ and intercept of $\frac{1}{k_2 q_e^2}$.

The kinetics studies were performed by mixing the ceria coated MNPs with a MB solution of known initial concentration and then taking UV-vis measurement at time intervals to quantify the change in concentration. From this, the % removal *versus* time can be plotted (Fig. S23†) or the $q(t)$ *versus* time (which has the same shaped curve). From this data then the linearized kinetic models can be plotted for the pseudo first order (Fig. S24†) and the pseudo second order (Fig. S25†) to derive the relevant constants.

The table below (Table 1) gives the results of this analysis. According to the R^2 analysis, the adsorption follows the second order model. The linearization of models, the fitting of the data

and the resultant coefficient of determination, R^2, should however be taken with caution when using different models as it introduces uncertainty and biasness that can skew results.[45] It is interesting to note that at lower concentrations the removal efficiency of the ceria coated magnetic nanoparticles is higher, which shows that the removal efficiency is dependent on the concentration of the MB solution.

Isotherm adsorption analysis of MB onto the ceria coated particles

The adsorption isotherms for this system were constructed in order to relate the sorbate concentration in the bulk and the adsorbed amount at the interface. Isotherms can also be used to indicate the distribution of dye molecules between the solid phase and the liquid phase. The Langmuir and Freundlich isotherms are well known models for adsorption that were constructed to determine which of the two best describes the adsorption of MB dye onto the ceria-coated MNPs.[2]

The Langmuir isotherm[47] is a theoretical model that is used to describe the equilibrium between sorbate and adsorbent system in a gas–solid system, where the adsorption of the sorbate is limited to one molecular layer at or before a partial pressure of unity is reached. The model can be transferred to a liquid–solid system using dye concentrations instead of partial pressure. The Langmuir isotherm model is represented by

$$q_e = \frac{q_m K_L C_e}{1 + K_L C_e}$$

where q_e is the mass of MB adsorbed per unit weight of adsorbent at equilibrium ($\text{mg}\ \text{g}^{-1}$), q_m is the maximum adsorption capacity to form a monolayer ($\text{mg}\ \text{g}^{-1}$), C_e is the equilibrium concentration of MB in solution ($\text{mg}\ \text{L}^{-1}$) and K_L is the Langmuir constant. Linearization of this equation to the $y = mx + c$ form gives

$$\frac{C_e}{q_e} = \frac{C_e}{q_m} + \frac{1}{K_L q_m}$$

Then by plotting $\frac{C_e}{q_e}$ against C_e, then q_m and K_L (the Langmuir constants) can be determined from the slope and intercept.

On the other hand, the Freundlich isotherm[48] is an empirical model that is based on multilayer adsorption and heterogeneous surface energy distribution. This model is described by the equation below,

Table 1 Kinetic data analysis results for 50 mg MNPs and 200 mL MB solution

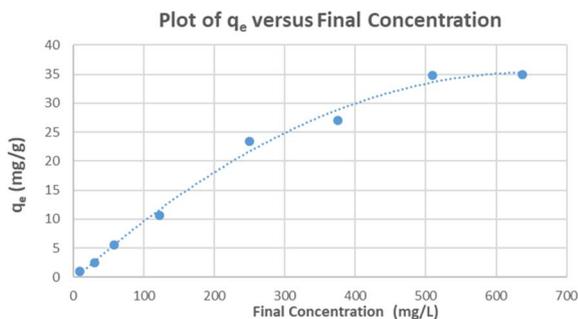| MB initial concentration (mg L^{-1})	First order			Second order			% MB removed
	q_e (mg g^{-1})	k_1 (min^{-1})	R^2	q_e (mg g^{-1})	k_2 (min^{-1})	R^2	
2	2.18	0.25	0.825	2.71	1.08	0.999	25
6	2.55	0.28	0.94	4.82	0.97	1	16
10	3.41	0.24	0.732	6.00	0.857	0.999	13

Paper

Fig. 5 Isotherm plot of the adsorption capacity and the equilibrium concentration.

Table 2 Langmuir and Freundlich constants derived by linearizing the models and fitting the data

Langmuir isotherm constants			Freundlich isotherm constants		
q_m (mg g^{-1})	K_L (L mg^{-1})	R^2	K_F	n	R^2
91.4	0.0011	0.800	0.141	1.13	0.989

$$q_e = K_F C_e^{\frac{1}{n}}$$

where q_e is the amount of solute that is adsorbed by the adsorbent at equilibrium (mg g^{-1}), K_F is the measure of the sorption capacity, n is the sorption intensity and C_e is the equilibrium concentration of MB in solution (mg L^{-1}). Linearization of this equation to the $y = mx + c$ form gives

$$\log(q_e) = \log(K_F) + \frac{1}{n}\log(C_e)$$

Then by plotting $\log(q_e)$ against $\log(C_e)$, then K_F and n (the Freundlich constants) can be determined from the slope and intercept.

The relationship between the adsorption capacity and its equilibrium concentration in aqueous solutions for the ceria-coated particles with MB was plotted (Fig. 5). Both of the linearized isotherms were plotted (Fig. S26 and S27†) and R^2 values of each of the isotherms and their parameters are summarized (Table 2). Although both isotherms yield a relatively linear relationship, when the coefficient of determination values (R^2) were taken into consideration as an indication of the goodness of fit of the data to a model, it implies that the Freundlich isotherm better describes the adsorption of MB dye onto the surface of the ceria-coated MNPs in comparison to the Langmuir isotherm. Again this result must be considered in context of having linearizing different models, as using different models introduces uncertainty and biasness that can skew results.[45]

As an example, the same data was processed using the solver function in Excel[49] with the non-linearized forms of both isotherms, where the residuals sum of squares (RSS) is an indication of the goodness of fit of the data, with the lower RSS indicating a better fit. The outcome of this processing (Table 3)

Table 3 Langmuir and Freundlich constants derived by fitting the data to the models by the residual sum of squares method

Langmuir isotherm constants			Freundlich isotherm constants		
q_m (mg g^{-1})	K_L (L mg^{-1})	RSS	K_F	n	RSS
47.7	0.0046	97.09	1.53	2.02	129.10

shows that in this case the Langmuir is a better fit with the lower RSS. The raw data used for these calculations is also given so that the statistically analysis can be repeated (Table S2†).

Recycling of the MNPs

The recyclability of the ceria-coated MNPs was tested in order to determine whether these particles could be reused for potential water remediation applications. The particles were recycled ten times and the percent MB removed was calculated from the UV-vis analysis using the Beer–Lambert law for each recycle. A plot of the % MB removal against the run number is show (Fig. S28†). As can be seen, the first run has the least removal of the MB. This could be because the ceria-coated particles had a material bound to the surface that was washed away with the first run. This is unusual though because the particles had been washed thoroughly and were calcined in the furnace prior to their first use. Another possible explanation is that the MB activate the surface on the first sorption and from then on, the surface is amiable to MB sorption. For 50 mg of the ceria coated nanoparticles in a 100 mL MB aqueous solution containing 8.9 mg L^{-1} (24 μM), the particles consistently removed approximately 60% of the MB for the runs 2–10. This equates to approximately 11.0 mg g^{-1}. This show that the removal efficiency is dependent on the concentration of the MNPs because previously when using a 200 mL MB aqueous solution containing 8.9 mg L^{-1} (24 μM) with 50 mg of MNPs, a calculation for the sorbent capacity gave 14.6 mg g^{-1} at that concentration of MNPs. The particles were magnetically extracted after the adsorption, placed in a vacuum oven to remove excess water and placed in a furnace at 400 °C for 7 hours to burn off the MB. After this, the ceria-coated nanoparticles were used directly in the next MB extraction run. The consistent MB removal after several runs shows that these nanoparticles have the potential for practical applications such as water purification to remove MB from wastewater, without the degradation of MB into other products.

MB dye is a cationic dye. It will have favourable electrostatic interaction with a negatively charged surface. Zeta potential analysis of the CeO$_2$ coated MNPs both before and after the first recycle shows that the particles have a small positive charge before and a small negative charge after the first recycle (Fig. S29 and S30†). This is a rationalisation why the first run of the dye extraction had a lower extraction compared with subsequent runs.

Conclusions

Thus, we have successfully synthesised magnetic core nanoparticles with a silica shell and an outer ceria shell. The

magnetic core was made by refluxing the precursors in ethylene glycol, the silica shell by the Stober method and the ceria shell by precipitation of CeO_2 onto the SiO_2 shell. These synthetic procedures were found to be easy to perform and reproducible. These particles were characterised by TEM, VSM and XRD techniques with these methods providing information about the morphology, the magnetisation and the phases present. The adsorption kinetics were analysed and the process was found to fit the pseudo second order model. An isotherm was plotted for the adsorption of MB and this was fitted to the Freundlich and Langmuir isotherm models with the best fit depending on the fitting procedure. The particles were tested for recyclability and were found to retain their ability to extract MB from aqueous solution even after ten recycles. These results indicate that these ceria-coated magnetic core nanoparticles may have application as new adsorbents for the removal of dyes from wastewater.

Experimental section

Starting materials

Iron(III) chloride hexahydrate, (reagent grade $\geq 98\%$), ethylene glycol, (anhydrous 98%), tetraethyl orthosilicate, (reagent grade 98%), HMTA (hexamethylene tetraamine), (reagent grade 99%), methylene blue, (>82% ACS reagent), ethanol, (HPLC grade), citric acid, (99%), trisodium citrate dihydrate, (>99% ACS reagent), have been supplied by Sigma-Aldrich. Ammonia solution, (25% analytical reagent grade), was supplied by Fisher Scientific. Manganese(II) chloride, (reagent ACS), was supplied by Riedel-de Haen. Sodium acetate, (extra pure >99%), was supplied by Merck. Cerium(III) nitrate hexahydrate, (extra pure 99.5%), was supplied by Fluka. MP water was prepared using a Millipore filtration system filtering distilled water. Ethanol (EtOH), methanol (MeOH) and acetone were technical grade solvents.

Instrumentation and characterisation techniques

For the instrumentation, the size and morphology of the particles were analyzed by TEM using the JEOL 2100 instrument operating at 200 kV. Samples were prepared by ultrasonically dispersing powder samples (approx. 5 mg) in ethanol (approx. 1.5 mL). One drop of the solution was placed onto a pure carbon TEM grid and the grid was then dried in air. ESI (electrospray ionization) mass spectra were acquired using a Bruker microTOF-Q III spectrometer interfaced to a Dionex UltiMate 3000 LC in positive and negative modes as required. The UV-visible spectra were obtained using Agilent Cary 60 spectrophotometer with a range of 1100–190 nm and a quartz cuvette with a pathlength of 1 cm and MP water was used as the solvent. X-ray powder diffraction was carried out using a Bruker, D2 Phaser 2nd generation, powder sample X-ray machine equipped with monochromatic high-intensity Cu-Kα radiation ($\lambda = 0.15406$ nm). All the XRD data obtained was background subtracted and it was ran between 2θ angles 15° to 85°. For obtaining magnetization measurements of the various dry products, an in-house assembled VSM was used at room temperature with field applied up to 1 T. The VSM was calibrated using a nickel sample of known mass. Nickel is

a ferromagnetic material, which has a known magnetic moment of 55.4 $Am^2\ kg^{-1}$ in an external field of 1 T at room temperature. FTIR spectra were obtained out using a PerkinElmer spectrum 100, equipped with a diamond window with an effective range of 4200–250 cm^{-1}. Brunauer–Emmett–Teller (BET) surface area analysis was carried out using a Nova 2400e Surface Area Analyzer (Quantachrome, UK) with nitrogen gas as the adsorbate. The sample was degassed for 1 hour at 200 °C under vacuum, prior to analysis. Zeta potential measurements were performed on a Malvern Zeta-Sizer Nano series instrument with a laser of 633 nm and scattering angle of 13°. EDX was performed on the JOEL 2100 with an Oxford Instruments 80 mm^2 XMAX EDX detector attached.

Preparation of manganese ferrite nanoparticles by polyol synthesis

$MnCl_2 \cdot H_2O$ (0.94 g, 4.8 mmol) was added to ethylene glycol (77.9 mL) in a 3-necked 250 mL RBF (round-bottom flask) and sonicated until the reagent was completely dissolved. A previously prepared solution of $FeCl_3 \cdot 6H_2O$ in ethylene glycol (12.9 mL, 0.74 M, 9.5 mmol) was added to the RBF and the reaction mixture was left sonicating for 5 minutes. The RBF was set up for mechanical stirring. A prepared solution of sodium acetate in ethylene glycol (19.6 mL, 2.44 M, 47.7 mmol) was added and the reaction mixture was left to stir for 5 minutes. The RBF was refluxed for 14 hours with the condenser open to air. Once the mixture has cooled to RT, the particles were magnetically extracted and they were then washed with methanol and MP water and stored in ethanol (22 mL) for further use.

Preparation of citrate-stabilized manganese ferrite ($MnFe_2O_4$@citrate)

$MnFe_2O_4$ MNPs in ethanol (1 g, 20 mL from previous) was added to a 500 mL RB and magnetically extracted. MP water (300 mL) was added and the solution was sonicated for 30 minutes. Trisodium citrate dihydrate (1.27 mL, 1.7 M, 2.17 mmol) was added to the NP solution and it was left to sonicate for 2 hours at 75 °C. Once the solution had cooled down to room temperature, the reaction mixture was neutralized using citric acid. The citrate-coated NPs were magnetically extracted, washed and stored in MP water (20 mL) for further use.

Preparation of silica-coated MNPs ($MnFe_2O_4$@SiO_2)

$MnFe_2O_4$@citrate (300 mg, 6 mL from previous) was added to a 1000 mL RBF and magnetically extracted. Ammonia (23 mL, 14.5 M), HPLC ethanol (736 mL) and MP water (184 mL) were added to the RBF and the reaction mixture was sonicated for 30 minutes. The RBF was placed in an ice bath to ensure the mixture was at RT prior to commencing the next step. The RBF was set up for mechanical stirring at room temperature under inert atmosphere. TEOS (0.557 mL, 2.5 mmol) was added to dry ethanol (20 mL) in a sample tube and the solution was transferred into a syringe. The TEOS solution was added to reaction mixture using a syringe pump (4 mL per hour) under inert atmosphere and it was left to mechanically stir overnight. The reaction mixture was neutralized to a pH of 7 using HCl (approx. 30 mL, 10 M) and a pH

meter. The product was magnetically extracted, washed and stored in a minimum amount of ethanol for further use.

Preparation of manganese ferrite@silica@ceria MNPs (MnFe$_2$O$_4$@SiO$_2$@CeO$_2$)

MnFe$_2$O$_4$@SiO$_2$ (450 mg) was added to a 3-necked 250 mL RBF and magnetically extracted. MP water (90 mL) was added to the RBF and it was left to sonicate for 30 minutes. Ce(NO$_3$)$_3$·6H$_2$O (1.05 g, 2.4 mmol) was added to the reaction mixture and the RBF was sonicated for 30 minutes to ensure that the reagent is fully dissolved. The RBF was placed in an ice bath and allowed to cool, followed by the addition of HMTA (4.73 g, 33.7 mmol) and the mixture was sonicated in ice for another 10 minutes. The RBF was set up for mechanical stirring and the mixture was left to stir overnight at room temperature. The reaction mixture was then heated to 70 °C for 2 hours and the product was magnetically extracted and washed using ethanol and MP water. The washed product was then calcined in the furnace at 400 °C for 4 hours.

Adsorption and kinetic analysis

A stock solution of MB (0.024 mM) was prepared. The ceria-coated MNPs (300 mg) were sonicated with 300 mL of this solution for 1 hour, the particles were magnetically extracted and placed in the furnace at 400 °C for 7 hours to activate the particles as previous work had found the first run to be lower than preceding recycles. The stock solution was diluted as need to make solutions of various concentrations for the kinetic studies. The adsorption studies were all carried out with 100 mL of MB solution with 25 mg of magnetic nanoparticles for 1 hour with sonication for 5 minutes and magnetic stirring for 55 minutes, with aliquots been taken at time intervals (5, 10, 15, 30, 45 and 60 minutes) to follow the change in concentration of the MB solution. A xenon arc lamp was used to illuminate the samples in both a quartz and borosilicate reaction vessel as required. For the isotherm studies MB solution of varying concentrations (10–650 mg L^{-1}) were made and adsorption studies carried out with 100 mL of the solution with 25 mg of MNPs. The MB adsorbed onto the respective MNPs at a given time, $q(t)$, was calculated as

$$q(t) = \frac{(C_I - C_F)V}{m}$$

where C_I is the initial concentration (mg L^{-1}), C_F is the final concentration (mg L^{-1}), V is the volume (L) and m is the mass of MNPs used (g). After the analysis, the MNPs from the aliquots were combined with the MNPs from the bulk solution and they were magnetically extracted to be recycled in the furnace at 400 °C for 7 hours. These nanoparticles were then used again in a further study.

Testing core–shell nanostructures for recyclability

MB solution (100 mL, 0.024 mM) was prepared and a UV-vis spectrum was obtained prior to addition to MNPs. MnFe$_2$O$_4$@SiO$_2$@CeO$_2$ (50 mg) and the MB solution were added to an RBF (250 mL), sonicated for 5 minutes and magnetically stirred for 55 minutes. After 1 hour the MNPs were magnetically extracted. A sample of this decanted solution was centrifuged (2500 rpm for 5 minutes). The UV-vis spectra of this sample was obtained ($\lambda_{max} \approx 664$ nm). The nanostructures were magnetically extracted and heated to 400 °C in the furnace for 7 hours to remove any residual MB. These MNPs were then used again in the same procedure as it was repeated nine more times and the obtained results were compared.

Conflicts of interest

There are no conflicts to declare.

Acknowledgements

References

1 M. A. Islam, I. Ali, S. M. A. Karim, M. S. Hossain Firoz, A.-N. Chowdhury, D. W. Morton and M. J. Angove, *J. Water Process Eng.*, 2019, **32**, 100911.

2 H. Shayesteh, A. Ashrafi and A. Rahbar-Kelishami, *J. Mol. Struct.*, 2017, **1149**, 199–205.

3 H. Xia, L. Chen and Y. Fang, *Sep. Sci. Technol.*, 2013, **48**, 2681–2687.

4 W. Driscoll, S. Thurin, V. Carrion, R. H. Steinhorn and F. C. Morin, *J. Pediatr.*, 1996, **129**, 904–908.

5 N. García Doménech, F. Purcell-Milton and Y. K. Gun'ko, *Mater. Today Commun.*, 2020, **23**, 100888.

6 M. A. Rauf, M. A. Meetani, A. Khaleel and A. Ahmed, *Chem. Eng. J.*, 2010, **157**, 373–378.

7 S. Raghu and C. Ahmed Basha, *J. Hazard. Mater.*, 2007, **149**, 324–330.

8 B. Yang, J. Zuo, X. Tang, F. Liu, X. Yu, X. Tang, H. Jiang and L. Gan, *Ultrason. Sonochem.*, 2014, **21**, 1310–1317.

9 O. S. G. P. Soares, J. J. M. Órfão, D. Portela, A. Vieira and M. F. R. Pereira, *J. Hazard. Mater.*, 2006, **137**, 1664–1673.

10 S. Zhou, Z. Du, X. Li, Y. Zhang, Y. He and Y. Zhang, *R. Soc. Open Sci.*, 2019, **6**, 190351.

11 N. O. Mainya, P. Tum and T. M. Muthoka, *Int. J. Sci. Res.*, 2015, **4**, 3185–3189.

12 S. Shylesh, V. Schünemann and W. R. Thiel, *Angew. Chem., Int. Ed.*, 2010, **49**, 3428–3459.

13 K. El-Boubbou, *Nanomedicine*, 2018, **13**, 929–952.

14 E. Peng, F. Wang and J. M. Xue, *J. Mater. Chem. B*, 2015, **3**, 2241–2276.

15 S. Laurent, S. Dutz, U. O. Häfeli and M. Mahmoudi, *Adv. Colloid Interface Sci.*, 2011, **166**, 8–23.

16 R. Massart, *IEEE Trans. Magn.*, 1981, **17**, 1247–1248.

17 T. Hyeon, Su S. Lee, J. Park, Y. Chung and H. Bin Na, *J. Am. Chem. Soc.*, 2001, **123**, 12798–12801.

18 H. Deng, X. Li, Q. Peng, X. Wang, J. Chen and Y. Li, *Angew. Chem., Int. Ed.*, 2005, **44**, 2782–2785.

19 J. Govan and Y. Gun'ko, *Nanomaterials*, 2014, **4**, 222–241.

20 Y. Zhai, J. Zhai, M. Zhou and S. Dong, *J. Mater. Chem.*, 2009, **19**, 7030.

21 S. Dey and G. C. Dhal, *Mater. Sci. Energy Technol.*, 2020, **3**, 6–24.

22 K. Yoshikawa, H. Sato, M. Kaneeda and J. N. Kondo, *J. CO2 Util.*, 2014, **8**, 34–38.

23 L. Yu, Y. Ma, C. N. Ong, J. Xie and Y. Liu, *RSC Adv.*, 2015, **5**, 64983–64990.

24 S. Kong, W. Zhang, S. Gao and D. Chen, *J. Exp. Nanosci.*, 2019, **14**, 107–115.

25 M. L. Surve, *Silica Coating of Gold Nanoparticles*, University of Missouri, 2003.

26 S. Xuan, Y. X. J. Wang, J. C. Yu and K. C. F. Leung, *Chem. Mater.*, 2009, **21**, 5079–5087.

27 Q. Jiang, L. H. Liang and D. S. Zhao, *J. Phys. Chem. B*, 2001, **105**, 6275–6277.

28 A. S. Gorkusha, S. V. Tsybulya, S. V. Cherepanova, E. Y. Gerasimov and S. N. Pavlova, *Materials*, 2022, **15**, 7642.

29 P. SCHERRER, *Math. Phys.*, 1918, **2**, 98–100.

30 M. Ishii, M. Nakahira and T. Yamanaka, *Solid State Commun.*, 1972, **11**, 209–212.

31 Y. H. Deng, C. C. Wang, J. H. Hu, W. L. Yang and S. K. Fu, *Colloids Surf., A*, 2005, **262**, 87–93.

32 S. Kralj, D. Makovec, S. Čampelj and M. Drofenik, *J. Magn. Magn. Mater.*, 2010, **322**, 1847–1853.

33 M. A. Dheyab, A. A. Aziz, M. S. Jameel, O. A. Noqta, P. M. Khaniabadi and B. Mehrdel, *Sci. Rep.*, 2020, **10**, 1–8.

34 W. Stöber, A. Fink and E. Bohn, *J. Colloid Interface Sci.*, 1968, **26**, 62–69.

35 A. P. Philipse, M. P. B. van Bruggen and C. Pathmamanoharan, *Langmuir*, 1994, **10**, 92–99.

36 J. Zou, Y. G. Peng and Y. Y. Tang, *RSC Adv.*, 2014, **4**, 9693–9700.

37 M. B. Gawande, Y. Monga, R. Zboril and R. K. Sharma, *Coord. Chem. Rev.*, 2015, **288**, 118–143.

38 V. Wells, A. Riaz, Q. Sun, X. Li, N. Yan, C.-H. Wang and W. Lipiński, *Appl. Phys. Lett.*, 2022, **120**, 143905.

39 Y. Deng, D. Qi, C. Deng, X. Zhang and D. Zhao, *J. Am. Chem. Soc.*, 2008, **130**, 28–29.

40 P.-L. Chen and I. Chen, *J. Am. Ceram. Soc.*, 1993, **76**, 1577–1583.

41 S. Brunauer, P. H. Emmett and E. Teller, *J. Am. Chem. Soc.*, 1938, **60**, 309–319.

42 E. P. Barrett, L. G. Joyner and P. P. Halenda, *J. Am. Chem. Soc.*, 1951, **73**, 373–380.

43 F. Huang, L. Chen, H. Wang and Z. Yan, *Chem. Eng. J.*, 2010, **162**, 250–256.

44 M. J. Hülsey, C. W. Lim and N. Yan, *Chem. Sci.*, 2020, **11**, 1456–1468.

45 E. D. Revellame, D. L. Fortela, W. Sharp, R. Hernandez and M. E. Zappi, *Clean. Eng. Technol.*, 2020, **1**, 100032.

46 Y. Ho and G. McKay, *Process Biochem.*, 1999, **34**, 451–465.

47 I. Langmuir, *J. Am. Chem. Soc.*, 1918, **40**, 1361–1403.

48 H. Freundlich and W. Heller, *J. Am. Chem. Soc.*, 1939, **61**, 2228–2230.

49 F. X. B. T.-C. E. McConville, *Chem. Eng.*, 2008, **115**, 48.